CSIRO PUBLISHING

Australian Journal of Physics

Volume 51, 1998

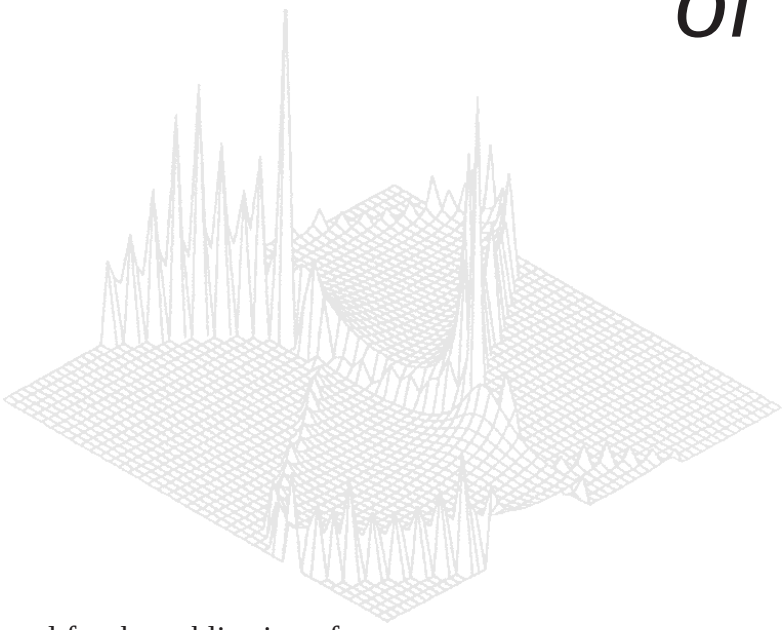

A journal for the publication of
original research in all branches of physics

www.publish.csiro.au/journals/ajp

All enquiries and manuscripts should be directed to
Australian Journal of Physics
CSIRO PUBLISHING
PO Box 1139 (150 Oxford St)
Collingwood Telephone: 61 3 9662 7626
Vic. 3066 Facsimile: 61 3 9662 7611
Australia Email: peter.robertson@publish.csiro.au

Published by **CSIRO** PUBLISHING
for CSIRO and the
Australian Academy of Science

Aust. J. Phys., 1998, **51**, 707–28

Application of DFT and EMS to the Study of Strained Organic Molecules*

W. Adcock,[A] *M. J. Brunger,*[A] *M. T. Michalewicz*[B] *and D. A. Winkler*[C]

[A] Departments of Chemistry and Physics, Flinders University of South Australia, GPO Box 2100, Adelaide, SA 5001, Australia.
[B] CSIRO Mathematical and Information Sciences, BOM/CSIRO High Performance Computing and Communication Centre, 24th Floor, 150 Lonsdale Street, Melbourne, Vic. 3000, Australia.
[C] CSIRO Division of Molecular Science, Private Bag 10, Clayton South MDC, Clayton, Vic. 3169, Australia.

Abstract

Electron momentum spectroscopy (EMS) studies of the valence shells of [1.1.1]propellane, 1,3-butadiene, ethylene oxide and cubane are reviewed. Binding energy spectra were measured in the energy regime of $3 \cdot 5$–$46 \cdot 5$ eV over a range of different target electron momenta, so that momentum distributions (MDs) could be determined for each ion state. Each experimental electron momentum distribution is compared with those calculated in the plane wave impulse approximation (PWIA) using both a triple-ζ plus polarisation level self-consistent field (SCF) wave function and a further range of basis sets as calculated using density functional theory (DFT). A critical comparison between the experimental and theoretical momentum distributions allows us to determine the 'optimum' wave function for each molecule from the basis sets we studied. This 'optimum' wave function then allows us to investigate chemically or biologically significant molecular properties of these molecules. EMS–DFT also shows promise in elucidating the character of molecular orbitals and the hybridisation state of atoms.

1. Introduction

Electron momentum spectroscopy (EMS), or (e, 2e) coincidence spectroscopy, is a tool for the investigation of the dynamic structure of molecules. It is quite unique in its ability to measure the momentum density of electronic orbitals for the ground state of a molecule (McCarthy and Weigold 1991). In a kinematically-complete ionisation reaction the differences between the observed final and initial total electron energies and momenta are respectively the energy eigenvalue of the corresponding state of the residual ion and the momentum of the struck electron at the collision instant. From an ensemble of ionisation events we observe the orbital momentum density for each ion state. The EMS technique and its theoretical analysis have been discussed in detail elsewhere (McCarthy and Weigold 1991; Coplan *et al.* 1994).

In this paper we present some results from experimental EMS studies of four small organic molecules: [1.1.1]propellane; 1,3-butadiene; ethylene oxide; and cubane. However, as detailed EMS and density functional theory (DFT) studies for two of these molecules have previously been reported (Adcock *et al.* 1995,

* Dedicated to Professor Erich Weigold on the occasion of his sixtieth birthday.

 10.1071/PH97092 0004-9506/98/040707$10.00

1997; Brunger *et al.* 1998), our focus in this review is the use of EMS coupled with density functional theory calculations to elucidate chemically interesting properties of these molecules.

2. Apparatus

A full description of the coincidence spectrometer and the method of taking the data can be found in McCarthy and Weigold (1988), although we note that since their report there has been a major upgrade in the data acquisition and computer control system (Adcock *et al.* 1997).

In the present work noncoplanar symmetric kinematics is employed with the two outgoing electrons having essentially equal energies and making equal polar angles ($\theta = 45°$) with respect to the incident electron beam. The incident electron energy E_0 was 1500 eV for butadiene and 1000 eV for propellane, ethylene oxide and cubane, plus the binding energy ϵ_f of the struck electron. The typical binding energy range of interest ($\epsilon_f = 3{\cdot}5 - 46{\cdot}5$ eV) is scanned by sequentially stepping through the entire set of azimuthal angles ϕ ($\phi = 0 - 25°$) using a 'binning' mode. Scanning through a range of ϕ is equivalent to sampling different target electron momenta p ($0{\cdot}1$–2 a.u.).

The coincidence energy resolution of the present work, as determined from measurements of the binding energy spectrum of helium, varied from $0{\cdot}6$ eV to $1{\cdot}6$ eV (FWHM) depending on the target gas under study. We note the lower bound value was recently achieved by monochromating the incident electron beam. In all cases the current of this electron beam was greater than 30 μA. The angular resolution was $\Delta\phi = 1{\cdot}2°, \Delta\theta = 0{\cdot}6°$, as determined from the electron optics and apertures and from a consideration of the argon 3p angular correlation. The analysis of the measured binding energy spectra has also been described many times before (see, for example, Adcock *et al.* 1997). Briefly, a least squares fit to the spectra (Bevington and Robinson 1990), assuming Gaussian profiles, is performed. The binding energies of the respective orbitals are usually fixed at the known photoelectron spectroscopy (PES) values, although satellite lines can complicate this, and the Gaussian widths are a convolution of the energy resolution and the natural line widths of the respective orbitals. The area under each profile, and its uncertainty, are determined in the fit.

Since the EMS technique is very sensitive to impurities, great care was exercised to minimise the possibility of sample contamination both during its synthesis (propellane and cubane) and in its transportation from the storage reservoir to the interaction region. The butadiene and ethylene oxide sources were commercially purchased with high purity. Note that the sample gas driving pressure was too low to cause any significant clustering by supersonic expansion. The results of each scan were carefully monitored for any signs of sample degradation and samples were regularly changed to additionally minimise the possibility of sample degradation.

3. Application of DFT to EMS

In the independent-particle (e.g. Hartree–Fock or density-functional) model each ion state corresponds to a molecular orbital. Normalisation of momentum density gives the orbital occupation number. Each independent-particle ion state

is split into a symmetry manifold by electron correlation, with each state of a symmetry manifold being identified by the shape of its momentum-density profile. The summed momentum density for the manifold is equal to the momentum density of the corresponding orbital. The fraction of the manifold momentum density belonging to an ion state is the spectroscopic factor (which sum to unity for each manifold).

The plane wave impulse approximation (PWIA) is used to analyse the measured cross sections for high-momentum transfer (e, 2e) collisions (McCarthy and Weigold 1988). Using the Born–Oppenheimer approximation for the target and ion wave functions, the (e, 2e) differential cross section σ for randomly-oriented molecules and unresolved rotational and vibrational states is given by

$$\sigma = K \int d\Omega |\langle p \Psi_f^{N-1} | \Psi_i^N \rangle|^2 \,,$$

where K is a kinematical factor which is essentially constant in the present experimental arrangement, Ψ_f^{N-1} and Ψ_i^N are the electronic many-body wave functions for the final ion and target ground states, and p is the momentum of the bound electron at the instant of ionisation. The $\int d\Omega$ denotes an integral over all angles (spherical averaging) due to the averaging over all initial rotational states.

The momentum-space target-ion overlap $\langle p \Psi_f^{N-1} | \Psi_i^N \rangle$ (Casida 1995) can be evaluated using configuration interaction (CI) descriptions of the many-body wave functions, but usually the weak-coupling approximation is made. Here, the target-ion overlap is replaced by the relevant orbital of, for example, the Hartree–Fock or Kohn–Sham (Kohn and Sham 1965) ground state Ψ_0, multiplied by a spectroscopic amplitude. This amplitude is the coefficient, in the CI description of the ion state, of the configuration representing a hole in the appropriate ground state orbital. With these approximations, the above integral in σ reduces to

$$\sigma = K S_j^{(f)} \int d\Omega |\phi_j(p)|^2 \,,$$

where $\phi_j(p)$ is the momentum space orbital. The spectroscopic factor $S_j^{(f)}$ is the square of the spectroscopic amplitude for orbital j and ion state f. It satisfies the sum rule

$$\sum_f S_j^{(f)} = 1 \,.$$

Hence, it may be considered as the probability of finding the one-hole configuration in the many-body wave function of the ion.

The Kohn–Sham equation (Kohn and Sham 1965) of DFT may be considered as an approximate quasiparticle equation, with the potential operator approximated by the exchange-correlation potential (Casida 1995). The quasiparticle energies are given by the poles in the Green function of this equation, which can be evaluated using diagrammatic perturbation theory (von Niessen *et al.* 1984). An

example of this calculation, which omits diagrams above the third order, is the third-order algebraic diagrammatic construction, or ADC(3), method.

Recently, the physical significance of the valence orbitals of DFT has been validated by their ability to describe EMS data that are not well described by SCF calculations which omit electron-correlation considerations, but are well described by full CI calculations (Duffy *et al.* 1994). Brion's group (e.g. Brion 1993, 1995; Zheng *et al.* 1995; Neville *et al.* 1996) have also shown that Kohn–Sham DFT calculations provide better agreement with experiment for the frontier orbitals of glycine and dimethoxymethane than even the near Hartree–Fock limit results. Their results indicate that electron correlation effects are an important factor in describing the chemically sensitive outer spatial (low momentum) regions of the highest occupied molecular orbital (HOMO) electron densities.

In order to compute the coordinate-space Kohn–Sham orbitals ϕ_j, we employed the DFT program DGauss (Andzelm and Wimmer 1992; Komornicki and Fitzgerald 1993). The molecular coordinates at the optimum geometry (minimum energy) and the Gaussian molecular orbital parameters (coefficients and exponents) were next treated as an input to the Flinders-developed program AMOLD, which computes the momentum space spherically-averaged molecular-structure factor (Michalewicz *et al.* 1995) and the (e, 2e) cross section or momentum distribution. The comparisons of calculated MDs with experiment may be viewed as an exceptionally-detailed test of the quality of the basis set.

In our studies we have used a number of basis sets in the computations: SCF (Snyder and Basch 1972); SCF (von Niessen *et al.* 1984); DFT (DZ94); DFT (DZ94P); DFT (DZVP); DFT (DZVP2); DFT (TZ94); DFT (TZ94.bspp; DFT (TZ94P); DFT (TZVP). Here DZ and TZ denote basis sets of double-, or triple-ζ quality, while V denotes a calculation in which such a basis is used only for the valence orbitals and a minimal basis is used for the less-chemically-reactive orbitals. The inclusion in the basis of long-range polarisation functions is denoted by P. An improvement over the local-density approximation (LDA) or the local-spin-density (LSD) approach to approximating the exchange-correlation functional can be obtained by using functionals that depend upon the gradient of the charge density (Becke 1988*a*, 1988*b*; Perdew 1986; Lee *et al.* 1988; Stoll *et al.* 1978). In our study, we used several different approximations (BP, bspp or BLYP) to the exchange-correlation energy functional. The nonlocal density-gradient correction for the nonlocal models was applied self-consistently throughout the entire computations.

4. Chemical Significance of EMS

Electron momentum spectroscopy provides a sensitive probe of molecular structure, chemical bonding and reactivity in the chemically important outer spatial regions of the electron distribution. To chemists, EMS is of considerable interest for three principal reasons:

(i) EMS offers the intriguing possibility of imaging molecular orbitals. As Coplan *et al.* (1996) stated '... momentum densities are only a phase factor and Fourier transform away from the wave function from which all observable properties of atoms and molecules can, in principle, be obtained'.

(ii) Within the plane wave impulse approximation (PWIA) and, in many cases, the target Hartree–Fock (THFA) approximation, this measured momentum cross section may be directly compared with the calculated spherically averaged MD of a specific molecular orbital, once the appropriate angular-resolution function has been folded in (Frost and Weigold 1982). Hence, EMS is also a powerful technique for evaluating the quality of theoretical wave functions in quantum chemistry (Bawagan *et al.* 1987; Zheng *et al.* 1995).

(iii) It is of considerable interest to use EMS to study properties of molecules with unusual characteristics such as strained geometries and unusual hybridisations or electronic properties. EMS coupled with DFT calculations may elucidate significant molecular features difficult to study by other techniques.

Chemical considerations influenced the choice of the four small molecules studied: [1.1.1]propellane, 1,3-butadiene, ethylene oxide and cubane (see the Scheme below). Propellane and cubane, containing unusual bonding or atom hybridisation, are likely to be a more stringent test of basis set quality. Ethylene oxide enables the effects of heteroatom substitution to be probed and butadiene introduces unsaturation and conjugation of double bonds into the study regime.

5. [1.1.1] Propellane

[1.1.1]propellane (Wiberg and Walker 1982; Wiberg 1983) is a truly remarkable hydrocarbon with 'inverted' geometries at the bridgehead carbon atoms which consequently has been the subject of experimental and theoretical studies of its properties (Wiberg 1984). The structure (Hedberg and Hedberg 1985), vibrational spectrum (Wiberg *et al.* 1985, 1992), total energy, strain energy (Wiberg *et al.* 1987*a*), and heat of formation have all been investigated and a study into its low-energy electron impact spectroscopy has also been reported (Schafer *et al.* 1992). The compound was found to be remarkably stable and to have a surprisingly short bridgehead C1–C3 bond length (160 pm, 9 pm longer than in cyclopropane), considering the extreme deviation from tetrahedral geometry and the anticipated steric strain.

The outervalence structure of [1.1.1]propellane has been previously studied with photoelectron spectroscopy (PES) using He(I) radiation by Honegger *et al.* (1985). We published the only previous EMS studies of [1.1.1]propellane (Adcock *et al.* 1995, 1997) which reported experimental binding energy spectra at two azimuthal angles, $\phi = 0°$ and $10°$, and MDs for its complete valence electronic structure. Details of the synthesis of [1.1.1]propellane and the experimental conditions used to measure the EMS spectra are reported therein.

By comparing the experimental and theoretical MDs, for the relevant valence orbitals, we can independently determine which of the SCF or DFT basis sets of states we have studied provides the most physically reasonable representation of the [1.1.1]propellane molecule. We utilise this optimum wave function to extract the chemically important molecular property information for the [1.1.1]propellane system including bond lengths, bond orders, and the state of hybridisation of the bridgehead carbon atoms.

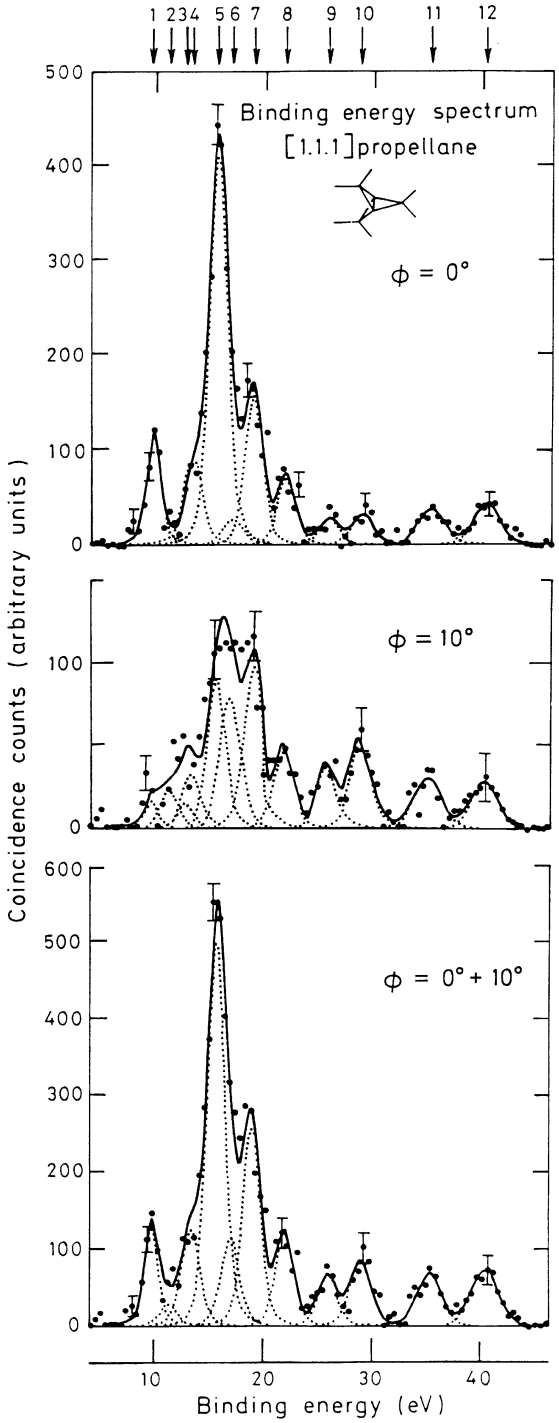

Fig. 1. Typical binding energy spectra from our 1000 eV noncoplanar symmetric EMS investigation into [1.1.1]propellane. The curves show the fits to spectra at $\phi = 0°, \phi = 10°$ and $\phi = 0° + 10°$ using the known energy resolution function.

Typical binding energy spectra of C_5H_6 in the region of 3·5–46·5 eV and at a total energy of 1000 eV are given in Fig. 1. Subsequent analysis allowed us to derive the required momentum distributions for the respective valence states of [1.1.1]propellane.

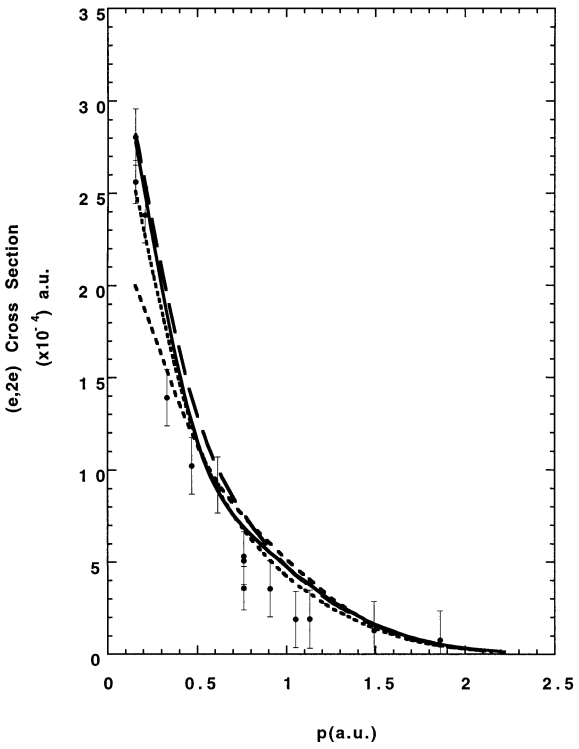

Fig. 2. The 1000 eV noncoplanar symmetric MD for the $3a_1'$ state of [1.1.1]propellane. The data of Adcock *et al.* (1997) (•) are compared against the results of our PWIA-SCF triple zeta basis (—), PWIA-DFT 6–31G Pople basis (- - -), and PWIA-DFT TZ94.bspp basis (– – –) calculations. Also shown is the result of the PWIA-DFT TZ94.bspp basis (-- --- --) scaled by a factor of 0·89.

Fig. 2 compares our experimental momentum distribution for the HOMO, $3a_1'$ state (peak 1 of Fig. 1) at $\epsilon_f = 9{\cdot}7$ eV of C_5H_6 with a small selection of the results from our PWIA-SCF and PWIA-DFT calculations. It is clear from Fig. 2 that the measured momentum distribution for the $3a_1'$ state is strongly peaked at smaller values of p. Historically, with the development of EMS, those orbitals which are symmetric in coordinate space have high (e, 2e) cross sections at small p. They are usually referred to as being 's-like' in nature. Thus, with respect to propellane, the result of Fig. 2 implies that this HOMO is 's-like'. All of the theoretical PWIA-SCF and PWIA-DFT results are consistent with this observation, although it is also apparent from Figure 2 that the 6–31G Pople basis results in a momentum distribution which seriously underestimates the measured (e, 2e) cross section at small p. On the other hand, both the TZ94P.BP and TZ94P.bspp basis sets (not plotted) lead to a calculated (e, 2e) cross section which is too large, compared to the experimental result, at small values of p ($\sim$0·16 a.u.). If the result for the TZ94.bspp basis calculation is scaled by our previously determined ADC(3) level spectroscopic factor (Adcock *et al.* 1995) for the $3a_1'$ state (0·89), then the level of agreement between the experimental and theoretical momentum distributions is good.

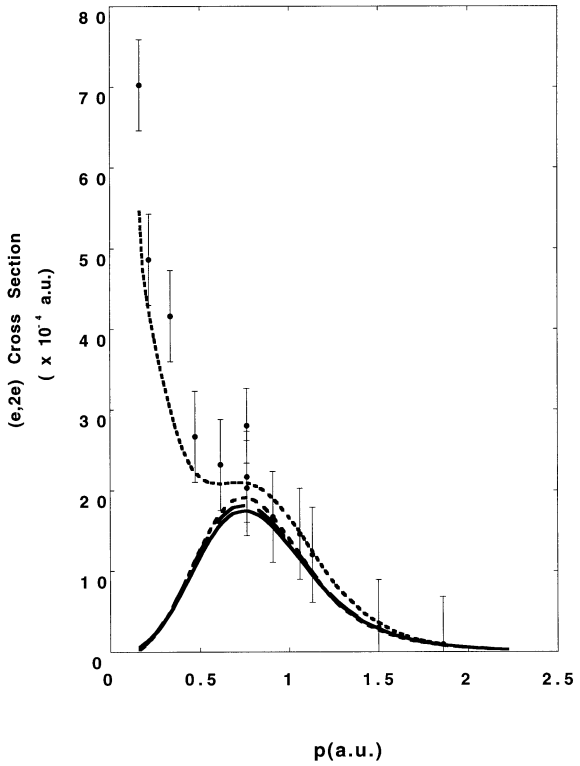

Fig. 3. The 1000 eV noncoplanar symmetric MD for the 2e′ state of [1.1.1]propellane. Legends are the same as in Fig. 2. Also shown is the result for the PWIA-DFT TZ94.bspp basis (-- --- --) when a $(0\cdot55)2a_1'$ pole strength contribution is added to that for the 2e′ state.

Fig. 3 shows the experimental momentum distribution for the 2e′ orbital (peak 5 of Fig. 1), at binding energy $\epsilon_f = 15\cdot7$ eV, along with our theoretical PWIA-SCF and PWIA-DFT results. Clearly none of the calculations, for any of the basis sets considered, provides an (e, 2e) cross section in agreement with the experimental result. This is particularly apparent for momenta less than $0\cdot76$ a.u., where the measured cross section starts to increase in value until reaching a maximum at $p \sim 0\cdot16$ a.u., while all of the theoretical cross sections tend to 0 as p approaches $0\cdot16$ a.u. Note that in this case orbitals which are anti-symmetric in coordinate space have very small (0 if angular resolution effects are removed) (e, 2e) cross sections as $p \to 0$ a.u. Historically they are referred to as being 'p-like' in nature. For $p > 0\cdot76$ a.u. there is fair agreement between all the 2e′ orbital PWIA-SCF and PWIA-DFT calculation results and the experiment. Previously (Adcock *et al.* 1995) we found from our ADC(3) calculation that the $2a_1'$ orbital was severely split, with a significant $2a_1'$ pole strength ($S_{2a_1'}^{ADC(3)} = 0\cdot39$) at almost the same binding energy as that of the 2e′ orbital. If we now allow for some $2a_1'$ flux in our PWIA-DFT calculation (55% contribution allowed here) using the TZ94.bspp basis, then very good qualitative agreement was found between theory and experiment for this combined momentum distribution [Fig. 3 for the

$2e' + (0{\cdot}55)2a_1'$ states MD]. Obviously the level of agreement for the (e, 2e) cross section, between the theory result that incorporates a $2a_1'$ contribution to the $2e'$ state and the measured data is still not perfect, perhaps reflecting a limitation in our $2a_1'$ orbital. Nonetheless this agreement is still quite good with that analysis providing the first unequivocal supporting evidence for the ADC(3) $2a_1'$ orbital spectroscopic strength splitting result of Adcock *et al.* (1995). We also analysed the MDs for all other states of [1.1.1]propellane and a detailed analysis was reported in Adcock *et al.* (1997).

The nature of the C1–C3 bridging bond in [1.1.1]propellane is rather controversial (Slee 1988). It is not clear whether there is a bridging bond at all, and if so, how it can be described. Attempts to describe the character of the bridging bond of [1.1.1]propellane have concentrated on: orbital theories, either to describe the bonding as predictive models, or as a means of analysing *ab initio* wave functions; electron density (Wiberg *et al.* 1987*b*) or related quantities. The studies of hybridisation in [l.m.n]propellanes performed by several workers gave contradictory results for [1.1.1]propellane, the most-strained example (Newton and Schulman 1972; Jarret and Cusumano 1990; Herr 1977).

Newton and Schulman (1972) noted that 'the electron density in the interbridgehead region is little different from that in bicyclo[1.1.1]pentane, a compound in which no formal bridgehead–bridgehead bond exists'. Electron-density difference maps also appeared to support this conclusion, since they showed a region of charge depletion between the bridgehead carbons, just as they do for the bicyclo calculations. A later orbital analysis of an *ab initio* wave function was performed by Jackson and Allen (1984). They focused on the valence canonical molecular orbitals and decomposed them using an interaction scheme between a C2 fragment and the outer parts of the rings (CH_2 groups). The HOMO was found to result from the in-phase combination of $2p\sigma$ orbitals on the bridgehead carbons, which has substantial density in the contributing regions. Jackson and Allen claimed that this orbital 'contributed nil to holding C1 to C3' and instead ascribed the bridgehead bonding to a degenerate pair of orbitals that place the electron density off-axis.

In contrast, the analysis of the total electron density by Wiberg and co-workers (Wiberg *et al.* 1987*a*, 1987*b*) concluded that there is a qualitative difference between the electron density in the bridging region of [1.1.1]propellane and of the analogous bicyclic species, bicyclo[1.1.1]pentane. The latter showed a minimum in the centre of the region while the former showed a bond point (Slee 1988). In addition, in [1.1.1]propellane the value of the electron density ρ at the bond point (Wiberg *et al.* 1987*b*) is $0{\cdot}203\ a_0^{-3}$, while in bicyclo[1.1.1]pentane it is only $0{\cdot}098\ a_0^{-3}$ (Slee 1988). Wiberg *et al.* (1987*a*, 1987*b*) found that the HOMO does contribute to the bonding of the bridgehead carbons. Indeed one-third of the total electron density is due to the HOMO, with its principal contribution, at the bond point, being due to the overlap of 2s orbitals. The assignment by Jackson and Allen (1984) of the bonding as a result of off-axis density, and their claim that there is 'very little charge density along the C1–C3 line of centres' is at variance with this observation of a bond point in the geometrical centre of the [1.1.1]propellane molecule.

Our EMS and DFT experiments on propellane helped resolve this controversy. The optimum wave function was found to be TZ94.bspp which gave best agreement

between experimental and theoretical MDs. Using this basis set we calculated that the interbridgehead carbon–carbon distance was 1·59 Å, in excellent agreement with the experimental value of 1·596 Å. In relation to the interbridgehead region of [1.1.1]propellane we estimated the electron density and subsequently bond order, midway between the two bridgehead carbons. Our bond order for the interbridgehead bond in [1.1.1]propellane of 0·70 was very similar to the Wiberg value (Wiberg *et al.* 1987*b*) of 0·73. We also calculated the bond order for the corresponding region in bicyclo[1.1.1]pentane as 0·40 (zero electron density gives a bond order of 0·21 in this analysis), indicating little or no interbridgehead bond in this compound.

The nature of the hybridisation of the C1–C3 bond in [1.1.1]propellane has also been examined. Newton and Schulman (1972) found the hybridisation of the interbridgehead bond to be $sp^{4\cdot13}$. On the other hand, a more recent NMR study by Jarret and Cusumano (1990) found the hybridisation at the bridgehead carbons to have a much higher p character ($sp^{8\cdot6}$–$sp^{4\cdot8}$) in the three bonds forming the three bridgehead methylene bonds and much larger s character ($sp^{0\cdot5}$) for the hybrids forming the interbridgehead bond.

Our EMS studies contributed to the understanding of the character of bonding between the bridgehead carbon atoms and their hybridisation state. The $3a_1'$ HOMO has very strong 's character', due to strong s contributions from the bridgehead and methylene carbons. The bridgehead s contributions are in-phase (bonding). There is also a strong out-of-phase (bonding) bridgehead p contribution. The degenerate $1e''$ orbitals have p character. There is essentially no s contribution to the bridgehead, and the p contribution is bonding. The $3e'$ orbital has antibonding s and p contributions to the bridgehead, both of which are responsible for the p-like character of the $3e'$ momentum profile. The $1a_2'$ orbital has essentially no contribution from the bridgehead carbons. Our finding that the HOMO makes a substantial contribution to the interbridgehead bond is consistent with the very recent results of Kar and Jug (1996). The very 's-like' nature of the HOMO (Fig. 2) is not inconsistent with the observation of Jarret and Cusumano (1990) in respect to the hybrid nature of the interbridgehead bond.

6. 1,3-Butadiene

Butadiene is a prototypical conjugated organic molecule and is the smallest example where the possibility of conjugation of double bonds exists. We studied 1,3-butadiene using EMS to assess the effect of unsaturation on the momentum distributions and the ability of DFT calculations to reproduce MDs extracted from experiment. Detailed binding energy spectra, orbital momentum distributions and detailed analyses of the DFT calculations have been reported by us recently (Brunger *et al.* 1998). In this work the $1b_g$, $1a_u$, $7a_g$, $6b_u$, $6a_g$, $5b_u$, $5a_g$, $4b_u$, $4a_g$, $3b_u$ and $3a_g$ valence orbitals of trans 1,3-butadiene were studied.

The molecular orbital calculations used seven DFT basis sets and two SCF basis sets. The DFT calculations incorporated both the local density approximation (LDA) and additionally, non-local correlation functional corrections (BP and BLYP).

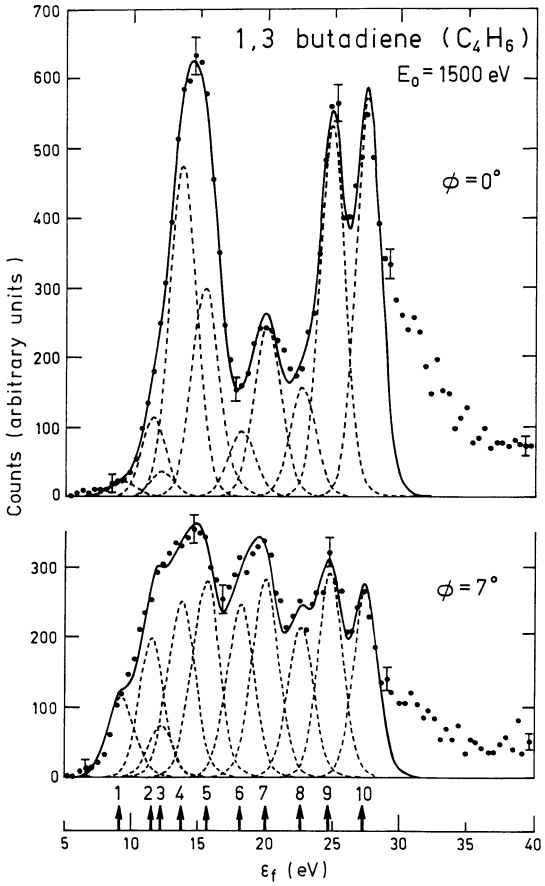

Fig. 4. Typical binding energy spectra from our 1500 eV noncoplanar symmetric EMS investigation into butadiene. The curves show the fits to spectra at $\phi = 0^\circ$ and $\phi = 7^\circ$ using the known energy resolution function.

Typical binding energy spectra of butadiene in the region ϵ_f = 5–40 eV are given in Fig. 4. As discussed earlier we used a least squares deconvolution method (Bevington and Robinson 1990) to derive the MDs for the respective valence states of trans 1,3-butadiene. The experimental momentum distribution for the HOMO, $1b_g$ state (peak 1 of Fig. 4) at $\epsilon_f = 9{\cdot}20$ eV is compared with PWIA-SCF and PWIA-DFT (LDA) calculations in Fig. 5. It is clear that the MD for the $1b_g$ state has very small flux at small values of p and a peak in the (e, 2e) cross section at $p = 0{\cdot}65$, implying that the HOMO is 'p-like' in character. This is clearly consistent with the HOMO being localised on the π system of the double bonds. All of the SCF and DFT results are consistent with the experimental MD although they all overestimate the magnitude of the cross section. When the results are scaled by a factor of $0{\cdot}65$ (the EMS spectroscopic factor for the $1b_g$ orbital at this ϵ_f), the agreement between theory and experiment is improved. The situation for the $7a_g$ orbital ($\epsilon_f = 12{\cdot}20$ eV) is quite different as Fig. 6 shows. Clearly the shapes of the SCF (Dunning 1971,

1989) and DFT(LDA) basis sets TZ94, TZVP, DZVP, DZVP2, DZ94 and DZ94P on the one hand, and the SCF (Snyder and Basch 1972) and DFT(LDA) TZ94P basis on the other, are completely different. The latter theoretical MDs are in good agreement with the experimental MDs. Again, scaling the TZ94P result by the ADC(3) spectroscopic factor improves the level of agreement. We analysed the MDs for the other states of 1,3-butadiene and a detailed report of this can be found in Brunger *et al.* (1998).

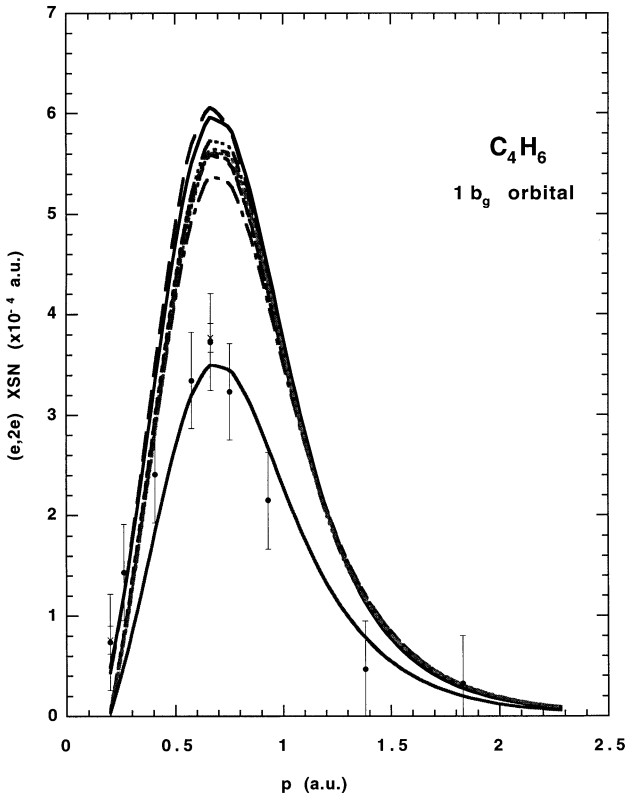

Fig. 5. The 1500 eV noncoplanar symmetric momentum distribution for the $1b_g$ state of butadiene. The data of Brunger *et al.* (1998) for runs A (●) and B (×) are compared against the results of our PWIA-SCF and PWIA-DFT (LDA) calculations: (—) Snyder and Basch (1972), (– -) Dunning (1971), (– – -) TZ94, (- - - - -) TZVP, (– - –) TZ94P, (- · - · -) DZVP, (- · · · ·) DZ94 and (- - - - - - -) DZ94P. Also shown is the 0·65× TZ94P (—) momentum distribution.

By comparing our measured and calculated momentum distributions for the valence states of trans 1,3-butadiene we concluded our 'optimum' wave function was TZ94P, i.e. a triple ζ quality wave function with extra polarisation. The determination of this wave function further allowed us to derive 1,3-butadiene's chemically interesting molecular properties, e.g. infrared spectra, bond orders, electron densities and many others (Brunger *et al.* 1998).

The results of our DFT calculations using the TZ94P basis set are in very good agreement with experimentally-determined molecular properties, and compare

favourably with the results from other MO calculations (Wiberg and Rosenburg 1990; Trætteberg and Hopf 1994) (Table 1). Delocalisation of the conjugated double bonds was evident from the deviations of the carbon–carbon bond lengths from their average values in simple, non-conjugated compounds, e.g. C=C 1·337 ± 0·006 Å and C–C 1·541 ± 0·003 Å (Lide 1990).

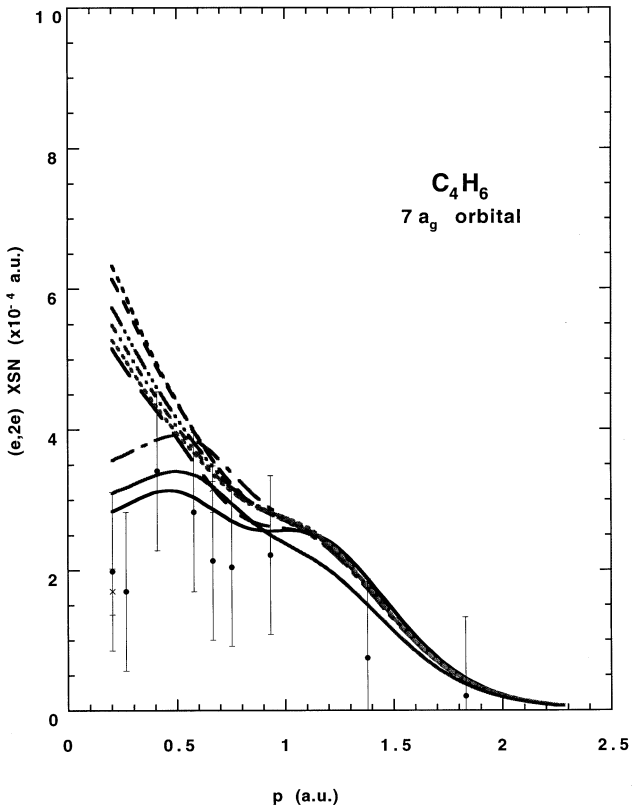

Fig. 6. The 1500 eV noncoplanar symmetric momentum distribution for the $7a_g$ state of butadiene. Legend is the same as Fig. 5 except now the 0·87× TZ94P (—) momentum distribution is shown.

We also investigated the electron density in the carbon–carbon bonding regions of 1,3-butadiene. We carried out a study analogous to that of Wiberg *et al.* (1987*a*, 1987*b*) to estimate the electron density (ρ_b) at the bond critical point. We obtained a value of $\rho_b = 0{\cdot}311a_0^{-3}$ for the C=C density and $0{\cdot}258a_0^{-3}$ for C–C density. We used Wiberg's empirical method to calculate bond orders, from DFT electron densities at the bond critical points, of 1·84 for the C=C bonds, and 1·27 for the C–C bonds. Lowdin population analysis yielded a C=C bond order of 1·63 and C–C bond order of 1·23, in good agreement with our values.

7. Ethylene Oxide

Ethylene oxide is the simplest heterocyclic molecule and has been widely studied by spectrocopic and theoretical methods. We report here a preliminary study of

Table 1. Selected molecular properties of 1,3-butadiene (acronyms are defined in the text)

Property	Experimental value	MP2/ 6-31G*[G]	MP2/ 6-31G*[D]	HF/ 6-31G*[D]	TZ94P[A]
$r_{C=C}$	1·341[C] 1·345(2)[F] 1·349(1)[E]	1·344	1·343	1·323	1·341
r_{C-C}	1·464[C] 1·465(3)[F] 1·467(2)[E]	1·458	1·456	1·468	1·446
r_{C-H}	1·090[C] 1·108(4)[F] 1·108(1)[E]		1·086av	1·076av	1·095av
−CCC (°)	123·3[C] 123·3(3)[F] 124·4(1)[E]	123·7	123·7	124·1	123·9
E (H)		−155·423	−155·442	−154·916	−154·548
Bond order C–C					1·23 Lowden 1·27 (ED)[B]
Bond order C=C					1·64 Lowden 1·83 (ED)[B]

[A] This work. [B] Derived from electron densities at bond critical points. [C] Bock and Panchenko (1989). [D] Wiberg *et al.* (1980). [E] Kveseth *et al.* (1980). [F] Landolt–Börnstein (a). [G] Traetteberg and Hopf (1994).

ethylene oxide using EMS and DFT. Ethylene oxide serves as a base molecule from which to explore the effects of hetero-atom substitution on momentum distributions and the adequacy by which they are simulated by PWIA-DFT calculations.

Fig. 7 shows the binding energy spectra at (*a*) $\phi = 0°$ and (*b*) $\phi = 10°$ for this molecule. As discussed previously binding energy spectra like this are then analysed and from this analysis the MDs for the valence orbitals are derived. The outermost valence (HOMO) $2b_2$ orbital (Fig. 8) is clearly 'p-like' in character and is quite well described by the DFT and SCF basis sets, with the exception of the PWIA-SCF description with Snyder and Basch (1972) basis which is clearly inadequate. From $\phi = 9 - 13°$ the cross sections predicted by DZ94, TZ94, TZ94P.bspp, TZ94P and DZVP2 are all slightly too large in magnitude.

The $2b_1 + 1a_2$ orbitals, which had to be summed due to energy resolution limitations, (Fig. 9) are not well described by any of the basis states, for momentum $\phi \leq 10°$. However, if a small (10%) $3a_1$ admixture is allowed for (see argument pertaining to this in Brunger *et al.* 1995) then the PWIA-SCF (Brunger *et al.* 1995) and PWIA-DFT (TZVP) MDs provide a very good description of the experimental MD. This implies that these basis states are providing a reasonable representation for the $2b_1$ and $1a_2$ orbitals.

Table 2 summarises the efficacy of the basis sets in reproducing the experimentally-derived ethylene oxide MDs. There is little to separate the PWIA-SCF calculation result of Brunger *et al.* (1995) from the present PWIA-DFT DZVP, TZVP results. As the total energy E (Hartrees) of the TZVP result is lower (more negative), therefore indicating a more stable configuration than the DZVP result, we can, on balance, choose it as our 'optimum' wave function for the C_2H_4O molecule.

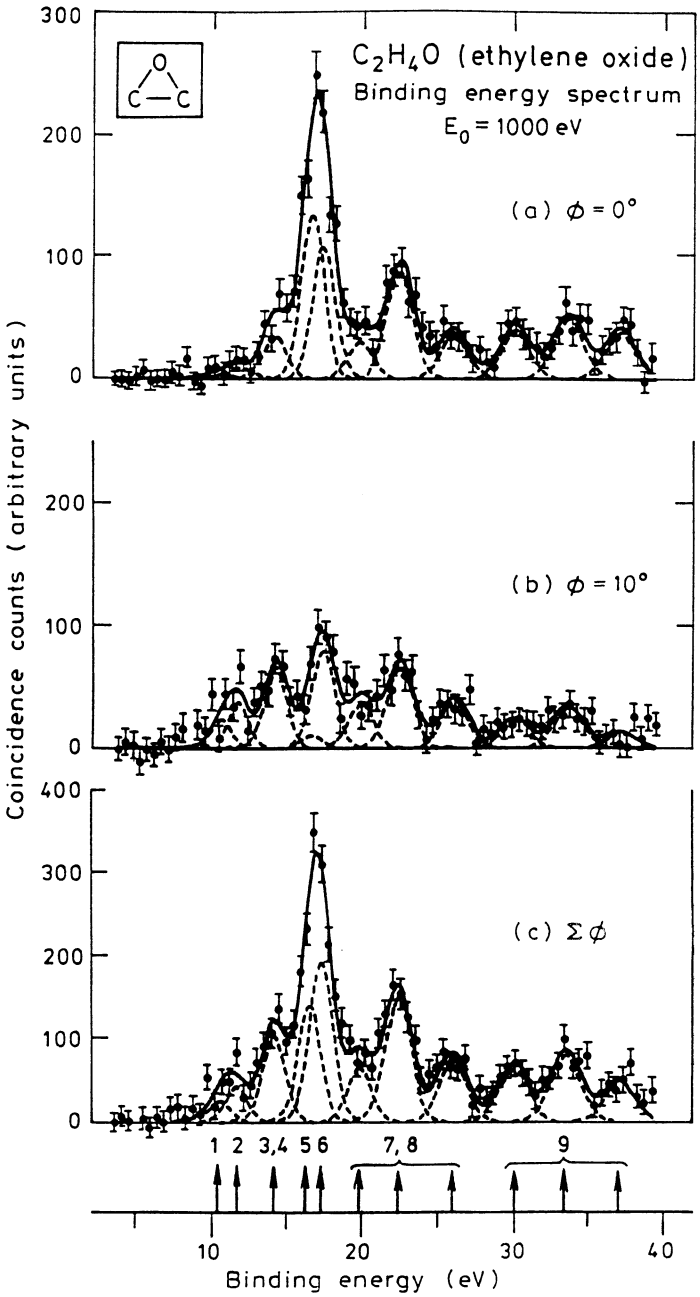

Fig. 7. The 1000 eV noncoplanar symmetric EMS binding energy spectra of ethylene oxide at (*a*) $\phi = 0°$, (*b*) $\phi = 10°$ and (*c*) $\phi = 0° + 10°$. The curves show the fitted spectra using the known energy resolution function.

Table 3 summarises molecular properties derived from our optimum basis function with experimental values. There is good agreement between the measured and calculated values for the heavy atoms with average deviations being generally

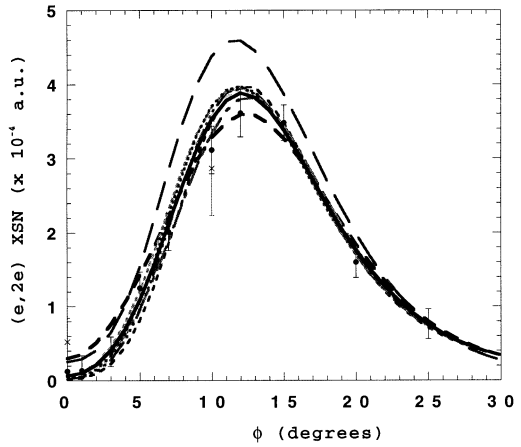

Fig. 8. The 1000 eV noncoplanar symmetric MD for the $2b_2$ state of ethylene oxide. The present data for runs A (●) and B (×) (Brunger *et al.* 1995) are compared against the results of our PWIA-SCF and PWIA-DFT (LDA) calculations: (—) Synder and Basch (1972), (– –-) Brunger *et al.* (1995), (– – – – –) DZ94, (-----) DZ94P, (— – –) DZVP, (– – – –) DZVP2, (— – – – –) TZ94,(-------) TZ94P.bspp (---------) TZ94P and (—) TZVP.

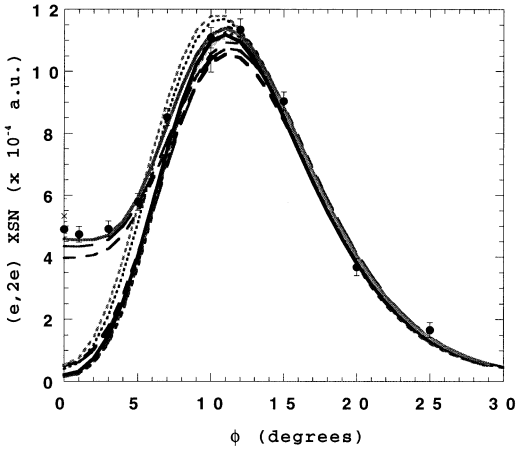

Fig. 9. The 1000 eV noncoplanar symmetric MD for the $2b_1 + 1a_2$ states of ethylene oxide. Legend is the same as Fig. 8 except now a 10% $3a_1$ contribution to Brunger *et al.* (1995) (—-), Snyder and Basch (1972) (– – -) and TZVP (—) MDs is also included.

less than 0·01 Å. The angles between the heavy atoms were in excellent agreement with the experimental values. The calculated and observed HCH and OCH angles only disagreed by slightly more than 1°. The calculated and measured values (Landolt–Börnstein (b)) for the total dipole moment were 2·01D, although such a high level of agreement is probably somewhat fortuitous.

Table 2. Level of agreement between experimental and theoretical MDs in ethylene oxide (acronyms are defined in the text)

G = good agreement, I = inadequate agreement and G/I = a marginal or doubtful level of agreement at least in some regions of the MD

Orbitals	SCF		DFT							
	SB	vN	DZ94	DZ94P	DZVP	DZVP2	TZ94	TZ94P.bspp	TZ94P	TZVP
$2b_2$	I	G/I	G/I	G	G	G/I	G/I	G/I	G/I	G
$4a_1$	I	G	I	G	G	G	I	G	I	G
$2b_1+1a_2$	I	I	I	I	I	I	I	I	I	I
$2b_1+1a_2+$ 10% $3a_1$ admixture	G/I	G	—	—	—	—	—	—	—	G
$3a_1+1b_2$	G/I	G	G	G	G	G/I	G/I	I	I	G
$1b_1+2a_1$	G	G	G	I	G	G	G	I	I	G
$1a_1$	G	G	G/I	G	G	G/I	G/I	G/I	G/I	G

Table 3. Some molecular property information on ethylene oxide (acronyms are defined in the text)

Property	Experimental value	TZVP.BP[A]
$r_{C–C}$ (Å)	$1{\cdot}466^{B}$ $1{\cdot}472^{C}$	$1{\cdot}476$
$r_{C–O}$ (Å)	$1{\cdot}431^{B}$ $1{\cdot}436^{C}$	$1{\cdot}444$
–HCH(°)	$116{\cdot}6^{B}$ $116{\cdot}7^{C}$	$115{\cdot}5$
–COC (°)	$61{\cdot}7^{C}$	$61{\cdot}4$
–OCH (°)	$114{\cdot}2^{C}$	$115{\cdot}3$
Bond order C–C		$1{\cdot}00$ Mayer $1{\cdot}04$ ED
Bond order C–O		$0{\cdot}96$ Mayer $1{\cdot}43$ ED

[A] This work. [B] Landolt–Börnstein (b). [C] Cunningham *et al.* (1951).

We also investigated the electron density in the bonding regions of ethylene oxide. As with [1.1.1]propellane and 1,3-butadiene we estimated the electron density ρ_b at the bond critical point. In this case we found them to be $0{\cdot}240\ a_0^{-3}$ for the C–C density and $0{\cdot}260\ a_0^{-3}$ for C–O density. This analysis yielded ethylene oxide bond orders of $1{\cdot}04$ for the C–C bonds, and $1{\cdot}43$ for the C–O bonds. Mayer population analysis yielded a C–C bond order of $1{\cdot}00$ and the C–O bond order of $0{\cdot}96$.

The infrared spectra of C_2H_4O and C_2D_4O are very complicated with almost all fundamental bands overlapping one another. This affects accurate measurements of vibrational frequencies and the interpretation of individual band intensities. Studies of the vibrational spectrum of ethylene oxide have been reported by several groups. Nakanaga (1980, 1981) reported the IR absorption intensities of ethylene oxide and ethylene oxide-*d*4 in the gas phase and compared these with the results of a CNDO/2 calculation. Spiekermann *et al.* (1982) carried out similar studies in the gas phase and reported the absolute IR intensities. Our TZVP.BP DFT basis set was able to calculate the frequencies of the vibrational

modes of ethylene oxide with reasonable accuracy and the calculated intensities of the transitions are in reasonable agreement with the observed experimental infrared spectra.

8. Cubane

Cubane, C_8H_8, is an unusual polycyclic molecule with carbon skeletal carbon bond angles near 90°, rather than 109·5° typical of acyclic systems. In fact, its endocyclic interorbital angles have been estimated to be 107° by NMR experiments, and 105° by x-ray crystallography. The molecule has unusual chemical properties such as a very high strain energy, carbon acidity (Alkorta and Elguera 1997) and kinetic stability. In addition cubane has potential as a scaffold for combinatorial chemistry, and as an energetic material precursor (Bashir-Hashemi *et al.* 1995; Lukin *et al.* 1997).

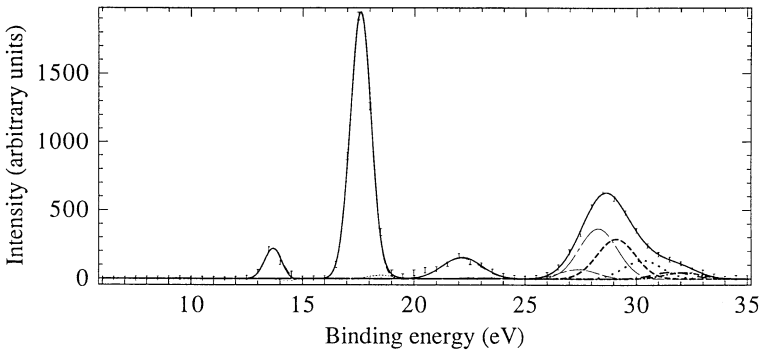

Fig. 10. Typical binding energy spectrum from our 1000 eV noncoplanar symmetric EMS investigation into cubane. The curves show the fit to the $\phi = 0°$ spectrum using the known energy resolution function.

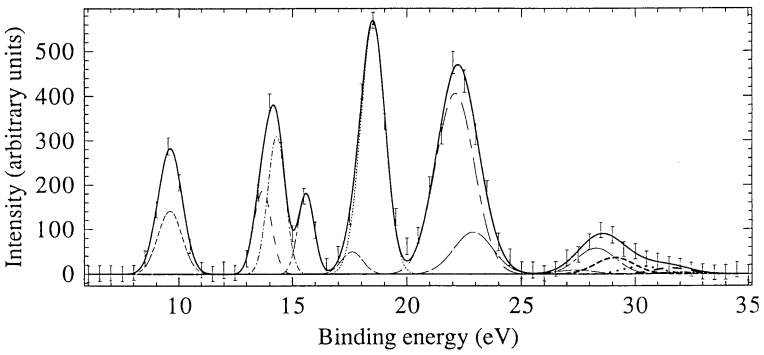

Fig. 11. Typical binding energy spectrum from our 1000 eV noncoplanar symmetric EMS investigation into cubane. The curves show the fit to the $\phi = 10°$ spectrum using the known energy resolution function.

We report here our first preliminary studies on cubane, which is also the first EMS study on this unique molecule. This is also the first EMS study using the recently developed (e, 2e) electron monochromator with improved coincidence energy resolution (0·6 eV FWHM) compared to earlier work ($> 1 \cdot 1$ eV). This

has enabled us to measure cleaner binding energy spectra, which has greatly improved our ability to interpret and analyse the EMS spectra, and derived MDs.

The binding energy spectra at $\phi = 0°$ and $\phi = 10°$ show that the inner valence $1t_{1u}$ and $1a_{1g}$ states (Figs 10 and 11) are split by final-state configuration-interaction effects. This is indicated by the need to use more than one Gaussian to fit the measured flux for each of these states. The spectra also clearly indicate the 's-like' and 'p-like' nature of the respective orbitals studied. The binding energy spectrum at $\phi = 0 + 10°$ is qualitatively similar to the corresponding PES spectrum (Bischof *et al.* 1978).

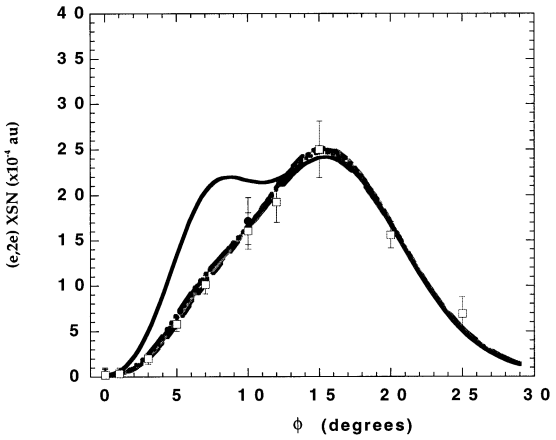

Fig. 12. The 1000 eV noncoplanar symmetric MD for the $2t_{2g}$ + $1t_{2u}$ outermost valence states of cubane. The present data for runs A (●) and B (□) are compared against the results of our PWIA-DFT (LDA) calculations: (—-) DZ94, (–--) DZ94P, (-----) DZVP, (—--) DZVP2, (—-----) TZ94, (—) TZ94P, and (---------) TZVP.

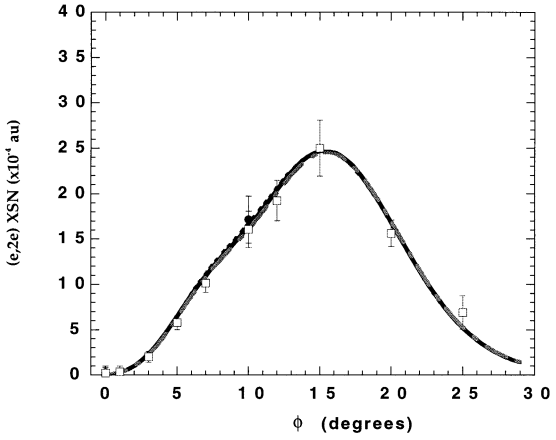

Fig. 13. The 1000 eV noncoplanar symmetric MD for the $2t_{2g}$ + $1t_{2u}$ outermost valence states of cubane. The present data for runs A (●) and B (□) are compared against the results of our PWIA-DFT TZVP calculations at the: LDA level (-------), BLYP level (—), and BP level (—--).

Figs 12 and 13 show our theoretical PWIA-DFT momentum distributions for the two outermost valence (degenerate) orbitals of cubane ($2t_{2g}$, $1t_{2u}$) and our corresponding experimental momentum distributions, as derived from our binding energy spectra. Clearly the TZ94P basis functions are totally inadequate representations of the $2t_{2g}+$ $1t_{2u}$ wave functions, particularly for momenta $\phi < 12°$. Fig. 13 shows that the PWIA-DFT result with TZVP basis functions is largely insensitive to whether LDA or BP and BLYP non-local functional corrections are used. This basis is in excellent agreement with experiment over all measured ϕ. A somewhat unexpected feature, compared to our usual (McCarthy and Weigold 1991) experience, is that these $2t_{2g}$ and $1t_{2u}$ wave functions 'p-like' outer valence orbitals have a peak in the cross section at a remarkably high value of ϕ, thereby indicating that they are rather delocalised in coordinate space. Our EMS measurements in cubane are now complete. Their analysis is underway with the aim again being to determine the optimum cubane wave function from those we have studied. Having achieved this we will use the optimum wave function to extract chemically interesting molecular properties for cubane.

9. Conclusions and Future Prospects

Using EMS techniques we have been able to assess *a priori*, for a number of different molecules and for the extensive range of basis states investigated, the quality of these basis states and therefore the validity of the physical representation provided by our respective basis functions. This procedure enabled us to select our optimum wave functions, in each case, from which the respective molecular properties were found to be in good accord with the available experimental data and other calculations. EMS–DFT shows considerable promise in helping to understand the character of molecular orbitals in organic molecules and the state of hybridisation of skeletal atoms.

Acknowledgments

We acknowledge the CSIRO Divisions of Mathematical and Information Sciences and Molecular Science for travel support. We thank Professors McCarthy and von Niessen for their continued interest in our work.

References

Adcock, W., Brunger, M. J., Clark, C. I., McCarthy, I. E., Weigold, E., Michalewicz, M. T., Winkler, D. A., and von Niessen, W. (1995). *Chem. Phys. Lett.* **244**, 433.

Adcock, W., Brunger, M. J., Clark, C. I., McCarthy, I. E., Michalewicz, M. T., von Niessen, W., Weigold, E., and Winkler, D. A. (1997). *J. Am. Chem. Soc.* **119**, 2896.

Alkorta, I., and Elguera, J. (1997). *Tetrahedron* **53**, 9741.

Andzelm, J., and Wimmer, E. J. (1992). *Chem. Phys.* **96**, 1290.

Bashir-Hashemi, A., Li, J., Gelber, N., and Ammon, H. (1995). *J. Org. Chem.* **60**, 698.

Bawagan, A., Brion, C. E., Davidson, E. R., and Feller, D. (1987). *Chem. Phys.* **113**, 19.

Becke, A. D. (1988*a*). *J. Chem. Phys.* **88**, 2547.

Becke, A. D. (1988*b*). *Phys. Rev.* A **38**, 3098.

Bevington, P. R., and Robinson, D. K. (1990). 'Data Reduction and Error Analysis for the Physical Sciences' (McGraw–Hill: New York).

Bischof, P., Eaton, P. E., Gleiter, R., Heilbronner, E., Jones, T. B., Musso, H., Schmelzer, A., and Stober, R. (1978). *Helv. Chim. Acta* **61**, 547.

Bock, C. W., and Panchenko, Y. N. (1989). *Theochem.* **56**, 69.

Brion, C. E. (1993). *In* 'The Physics of Electronic and Atomic Collisions' (Eds T. Anderson *et al.*), p. 350 (American Institute of Physics: New York).
Brion, C. E. (1995). *Science* **270**, 786.
Brunger, M. J., Weigold, E., and von Niessen, W. (1995). *Chem. Phys. Lett.* **233**, 214.
Brunger, M. J., Winkler, D. A., Michalewicz, M. T., and Weigold, E. (1998). *J. Chem. Phys.* **108**, 1958.
Casida, M. (1995). *Phys. Rev.* A **51**, 2005.
Coplan, M. A., Doering, J. P., Madison, D. H., Moore, J. H., and Pinkas, A. A. (1996). *Aust. J. Phys.* **49**, 321.
Coplan, M. A., Moore, J. H., and Doering, J. P. (1994). *Rev. Mod. Phys.* **66**, 985.
Cunningham, G. L., Boyd, A. W., Myers, R. J., Gwinn, W. D., and Le Van, W. I. (1951). *J. Chem. Phys.* **19**, 676.
Duffy, P., Chong, D. P., Casida, M., and Salahub, D. R. (1994). *Phys. Rev.* A **50**, 4707.
Dunning, T. H. (1971). *J. Chem. Phys.* **55**, 716.
Dunning, T. H. (1989). *J. Chem. Phys.* **90**, 1007.
Frost, L., and Weigold, E. (1982). *J. Phys.* B **15**, 2531.
Hedberg, L., and Hedberg, K. (1985). *J. Am. Chem. Soc.* **107**, 7257.
Herr, M. L. (1977). *Tetrahedron* **33**, 1897.
Honegger, E., Huber, H., Heilbronner, E., Dailey, W. P., and Wiberg, K. B. (1985). *J. Am. Chem. Soc.* **107**, 7172.
Jackson, J. E., and Allen, L. C. (1984). *J. Am. Chem. Soc.* **106**, 591.
Jarret, R. M., and Cusumano, L. (1990). *Tetrahedron Lett.* **31**, 171.
Kar, T., and Jug, K. (1996). *Chem. Phys. Lett.* **256**, 201.
Kohn, W., and Sham, L. (1965). *Phys. Rev.* **140**, A1133.
Komornicki, A., and Fitzgerald, G. (1993). *J. Chem. Phys.* **98**, 1398.
Kveseth, K., Seip, R., and Kohl, D. A. (1980). *Acta Chem. Scand.* A **34**, 31.
Landolt-Börnstein (*a*). New Ser. Group II, Vol. 7, p. 273 (Springer: New York).
Landolt–Börnstein (*b*). Neue Serie II/7, 3: 244, p. 185 (Springer: New York).
Lee, C., Parr, R. G., and Yang, W. (1988). *Phys. Rev.* B **37**, 785.
Lide, D. R (Ed.) (1990). 'Handbook of Chemistry and Physics', 71st edn, p. 9–1 (CRC Press: Boca).
Lukin, K. A., Li, J. C., Eaton, P. E., Kanomata, N., Hain, J., Punzalan, E., and Gilardi, R. (1997). *J. Am. Chem. Soc.* **119**, 9591.
McCarthy, I. E., and Weigold, E. (1988). *Rep. Prog. Phys.* **51**, 299.
McCarthy, I. E., and Weigold, E. (1991). *Rep. Prog. Phys.* **54**, 789.
Michalewicz, M. T., Brunger, M. J., McCarthy, I. E., and Norling, V. M. (1995). CRAY Users Group 1995 Fall Proceedings, Alaska (Ed. R. Shaginaw), pp. 37–41.
Nakanaga, T. (1980). *J. Chem. Phys.* **73**, 5451.
Nakanaga, T. (1981). *J. Chem. Phys.* **74**, 5384.
Neville, J. J., Zheng, Y., and Brion, C. E. (1996). *J. Am. Chem. Soc.* **118**, 10533.
Newton, M. D., and Schulman, J. M. (1972). *J. Am. Chem. Soc.* **94**, 773.
Perdew, J. P. (1986). *Phys. Rev.* B **33**, 8822.
Schafer, O., Allan, M., Szeimies, G., and Sanktjohanser, M. (1992). *J. Am. Chem. Soc.* **114**, 8180.
Slee, T. S. (1988). *In* 'Modern Models of Bonding and Delocalisation' (Eds J. F. Liebman and A. Greenberg), p. 63 (VCH Publishers: New York Weinheim).
Snyder, L. C., and Basch, H. (1972). 'Molecular Wavefunctions and Properties' (Wiley: New York).
Spiekermann, M., Bougeard, D., and Schrader, B. (1982). *J. Comput. Chem.* **3**, 354.
Stoll, H., Pavlidou, C. M. E., and Preuss, H. (1978). *Theor. Chim. Acta* **49**, 143.
Trætteberg, M., and Hopf, H. (1994). *Acta Chem. Scand.* **48**, 989.
von Niessen, W., Schirmer, J., and Cederbaum, L. S. (1984). *Comput. Phys. Rep.* **1**, 58.
Wiberg, K. B. (1983). *J. Am. Chem. Soc.* **105**, 1227.
Wiberg, K. B. (1984). *Acc. Chem. Res.* **17**, 379.
Wiberg, K. B., and Rosenburg, R. E. (1990). *J. Am. Chem. Soc.* **112**, 1509.
Wiberg, K. B., and Walker, F. H. (1982). *J. Am. Chem. Soc.* **104**, 5239.
Wiberg, K. B., Bader, R. F. W., and Lau, C. D. H. (1987*a*). *J. Am. Chem. Soc.* **109**, 985.

Wiberg, K. B., Bader, R. F. W., and Lau, C. D. H. (1987*b*). *J. Am. Chem. Soc.* **109**, 1001.
Wiberg, K. B., Dailey, W. P., Walker, F. H., Waddell, S. T., Crocker, L. S., and Newton, M. (1985). *J. Am. Chem. Soc.* **107**, 7247.
Wiberg, K. B., Rosenberg, R. E., and Waddell, S. T. (1992). *J. Phys. Chem.* **96**, 8293.
Zheng, Y., Neville, J. J., and Brion, C. E. (1995). *Science* **270**, 786.

Manuscript received 15 December 1997, accepted 11 March 1998